THE JOURNAL OF PHYSICAL CHEMISTRY B
A JOURNAL OF THE AMERICAN CHEMICAL SOCIETY

pubs.acs.org/JPCB Article

Probing Monomer and Dimer Adsorption Trends in the MFI Framework

Published as part of The Journal of Physical Chemistry virtual special issue "Carol K. Hall Festschrift".

Pavlo Kostetskyy, Elsa Koninckx, and Linda J. Broadbelt*

Cite This: *J. Phys. Chem. B* 2021, 125, 7199–7212 Read Online

ABSTRACT: Porous aluminosilicates such as zeolites are ubiquitous catalysts for the production of high-value and industrially relevant commodity chemicals, including the conversion of hydrocarbons, amines, alcohols, and others. Bimolecular reactions are an important subclass of reactions that can occur on Brønsted acid sites of a zeolite catalyst. Kinetic modeling of these systems at the process scale requires the interaction energetics of reactants and the active sites to be described accurately. It is generally known that adsorption is a coverage-dependent phenomenon, with lower heats of adsorption observed for molecules at higher coverage. However, few studies have systematically investigated the coadsorption of molecules on a single active site, specifically focusing on the strength of interaction of the second adsorbate after the initial adsorption step. In this work, we quantify the unimolecular and bimolecular adsorption energies of varying adsorbates, including paraffins, olefins, alcohols, amines, and noncondensible gases in the acidic and siliceous ZSM-5 frameworks. As a special case, olefin adsorption was examined for physisorption and chemisorption regimes, characterized by π-complex, framework alkoxide and carbenium ion adsorption, respectively. The effects of functional groups and molecular size were quantified, and correlations that relate the adsorption of the second adsorbate identity to that of the first adsorbate are provided.

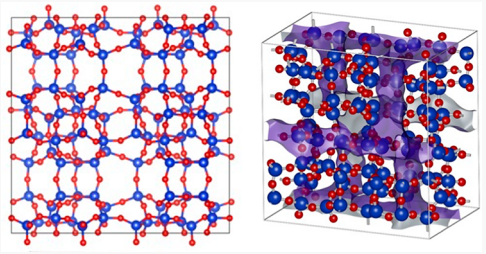

INTRODUCTION

Porous materials are critical components of most chemical processes at the industrial scale and include diverse classes of materials. Zeolites are a subclass of porous aluminosilicates, characterized by regular pore structure and shown to be stable for a wide range of operating conditions.[1] Zeolites are often used as molecular sieves and catalysts for processes including pollution adsorption,[2] gas separation,[3] biomass conversion,[4] and petrochemical upgrading.[5] There are over 200 known zeolite frameworks that have been characterized in terms of type of porosity, pore topology, and size distribution, among other properties.[6] Introduction of framework Al^{3+} ions and compensating H^+ species into the silica framework results in the formation of intraframework Brønsted acid (BA) sites. The total loading of framework aluminum (typically reported as the ratio of silicon to aluminum, Si/Al) correlates with the concentration of acid sites, with the extent of Al loading affecting total acid site concentration as well as porosity and crystallinity at the micro scale.

High-silica zeolites with Si/Al ratios in the thousands are manufactured at scale by replacing alumina contents with silica or by direct synthesis methods. High-silica zeolites are typically synthesized hydrothermally by heating a mixture composed of a (hydrated) silica source, a heteroatom source, an alkali hydroxide source, and a soluble organic species. The inorganic and organic components influence the development of zeolite phases and crystal morphology during synthesis.[7] Calorimetry and gravimetry were used in early experiments to determine the heat of adsorption into high-silica zeolites, usually in the form of silicalite. These early studies often compared the heats of adsorption of small molecules against various zeolite structures. In the 1990s, Dunne et al.[8] and Lee and Gorte[9] compared silicalite against acidic zeolites such as H-ZSM-5 and showed most adsorbates had higher differential heats on H-ZSM-5 compared to silicalite, suggesting a strong adsorption affinity for the Bronsted sites.[8,9] Similarly, Savitz et al. compared the adsorption of methane, ethane, and propane into a series of high-silica zeolites, showing that zero-coverage heats of adsorption are inversely proportional to pore diameter.[10] Chempath et al.[11] studied the adsorption of liquid phase alkane mixtures with experimental and computational tools, noting that long-chain alkanes have a siting preference for straight channels, while short hydrocarbons prefer to reside in the sinusoidal channels.

Received: March 31, 2021
Revised: June 2, 2021
Published: June 24, 2021

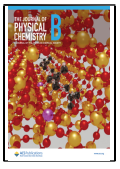

https://doi.org/10.1021/acs.jpcb.1c02929
J. Phys. Chem. B 2021, 125, 7199–7212

Catalytic and sorption applications of acidic zeolites have been examined for a range of chemical species with experimental and computational methods. A number of important experimental studies by Lercher and co-workers[12] reported experimental measurements of hydrocarbon adsorption in HZSM-5 through calorimetry and gravimetry studies. Adsorption enthalpies, maximum loading, and corresponding infrared signatures of adsorbed states were reported for different zeolite frameworks. Dispersion and van der Waals interactions were identified as primary contributions to the adsorption energy, reporting chain-length-dependent correlations. Gorte and co-workers similarly reported experimental calorimetry and temperature-programmed desorption (TPD) measurements of different adsorbate classes such as hydrocarbons, carbohydrates, H_2O, and light gases.[9,13] The total concentration and strength of BA sites were quantified through adsorption of probe molecules for different zeolite frameworks. Kotrel et al.[14] evaluated the catalytic cracking of hexane with acidic BEA, MFI, and FAU zeolites, highlighting the importance of intrapore stabilization of reactants and intermediates by medium-sized pore topologies.

Recent advances in synthetic techniques provide control over distribution of acid sites in the zeolite framework, including relative proximity to each other by utilizing structure-directing agents (SDA), resulting in materials with unique catalyst properties. Gounder and co-workers have successfully synthesized CHA zeolites with tuned acid site proximity and demonstrated significantly improved catalytic performance in methanol dehydration chemistry.[4b] Selective Al substitution may be achieved in other three-dimensional zeolite frameworks such as MFI through the utilization of SDA,[15] potentially providing access to tetrahedral positions previously considered to be less stable, such as T7, T9, and T11[16] in a paired site configuration.[15]

Conventional zeolite frameworks for which molecular adsorption has been an intense research focus include MFI, CHA, BEA, and FAU, among others.[3,8,10,13d,17] Adsorption processes are a critical part of catalysis, involving the interaction of adsorbates with catalytic active sites and with zeolite pore walls. In BA zeolites, these processes are characterized by electron transfer from the electron-rich adsorbate to the (relatively) electron-poor, framework-bound acidic proton.[18] In addition, weak interactions of adsorbates with internal pore walls and other adsorbates occur through dispersion and van der Waals interactions.[18b] In high-silica zeolites, these weaker van der Waals interactions are the only forces between the adsorbate and the framework molecules.

Modes of molecular adsorption in BA zeolites can be classified by the strength of interaction with the acid site and are generalized into chemisorption and physisorption, that is, strong and weak interactions, respectively.[13c] Adsorbate properties affect the strength of interaction, of which basicity (quantified as proton affinity (PA)) is most relevant and is defined as the gas phase binding energy of a proton. Additionally, molecular size and degree of branching are important considerations, especially for large molecules. Chemisorption in zeolites can thus be further distinguished by the extent of acid site deprotonation, with sufficiently basic (high PA) adsorbates capable of spontaneously stripping the proton from the active site and resulting in an acid−conjugate base pair, while adsorbates with low PA adsorb locally to the active site. Olefin adsorption is a special case among adsorbates considered in this work (Figure 1), with three distinct modes

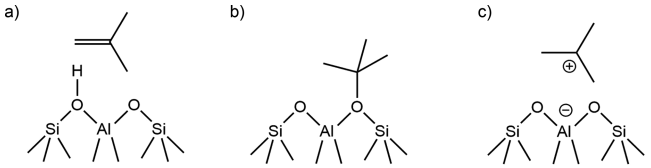

Figure 1. Graphical representation of olefin adsorption in acidic zeolites: (a) π-complexation, (b) alkoxide formation, and (c) carbenium ion formation, for isobutene as the sample adsorbate.

available, namely (a) (physisorbed) π-complex, (b) (chemisorbed) framework-bound alkoxide complex, and (c) gas-phase carbenium ion (specific to tertiary species).[19] It is important to note that only tertiary carbenium ions have been shown to be stable in the gas phase, with primary and secondary species forming surface-bound alkoxide complexes.

Molecular adsorption in zeolites is a coverage-dependent phenomenon, with higher adsorption energies observed at low coverage for both acidic and high-silica zeolites. For acidic zeolites, individual BA sites can accommodate multiple adsorbate molecules that are stabilized by local adsorbate−adsorbate and adsorbate−zeolite interactions. Well-known examples exhibiting these phenomena include hydrocarbon separations,[20] oligomerization,[21] dehydration,[22] esterification,[23] and other chemistries. In these cases, multimolecular adsorbate complexes are known to form, with the total number of adsorbates in the complex being a function of operating conditions.

Such coverage-dependent phenomena can be exemplified for hydrocarbons, carbohydrates, and noncondensible gases by experimental microcalorimetry measurements of Gorte et al.[8−10,13] For acidic zeolites, isosteric heats of adsorption decrease with increasing adsorbate loading, with sharp decreases in measured heats of adsorption observed once available BA sites have been titrated. Importantly, this adsorption behavior was not replicated in high-silica zeolites, with heats of adsorption remaining unchanged for small adsorbates such as methane and small increases in measured heats of adsorption for larger molecules such as propane for a range of loadings. This small increase was attributed to intrapore intermolecular interactions.

Acid-catalyzed hydrocarbon chemistry, such as olefin oligomerization, involves a large number of reactants, intermediates, and products that undergo different chemical transformations, of which many are bimolecular. Acid-catalyzed bimolecular reactions typically involve coadsorption of reactant molecules in close proximity on or near the same active site. Computational modeling of these systems is a powerful tool toward design, optimization, and scaleup of industrial-scale processes at a potentially lower cost relative to lab- and pilot-scale experiments. Kinetic models of such systems often involve networks of hundreds of interconnected elementary steps and rely heavily on scaling relations to estimate the relevant equilibrium and rate constants.[21]

Adsorption energies of molecules can be estimated from linear scaling relationships between adsorption energy and physicochemical properties of the adsorbing species;[24] however, these relations have been limited to monomer adsorption and constrained in applicability by zeolite and adsorbate identity, size, and shape. Computational tools such as electronic structure calculations are typically used to generate empirical scaling correlations that relate molecular properties to their reactivity for a specific catalyst.

https://doi.org/10.1021/acs.jpcb.1c02929
J. Phys. Chem. B 2021, 125, 7199−7212

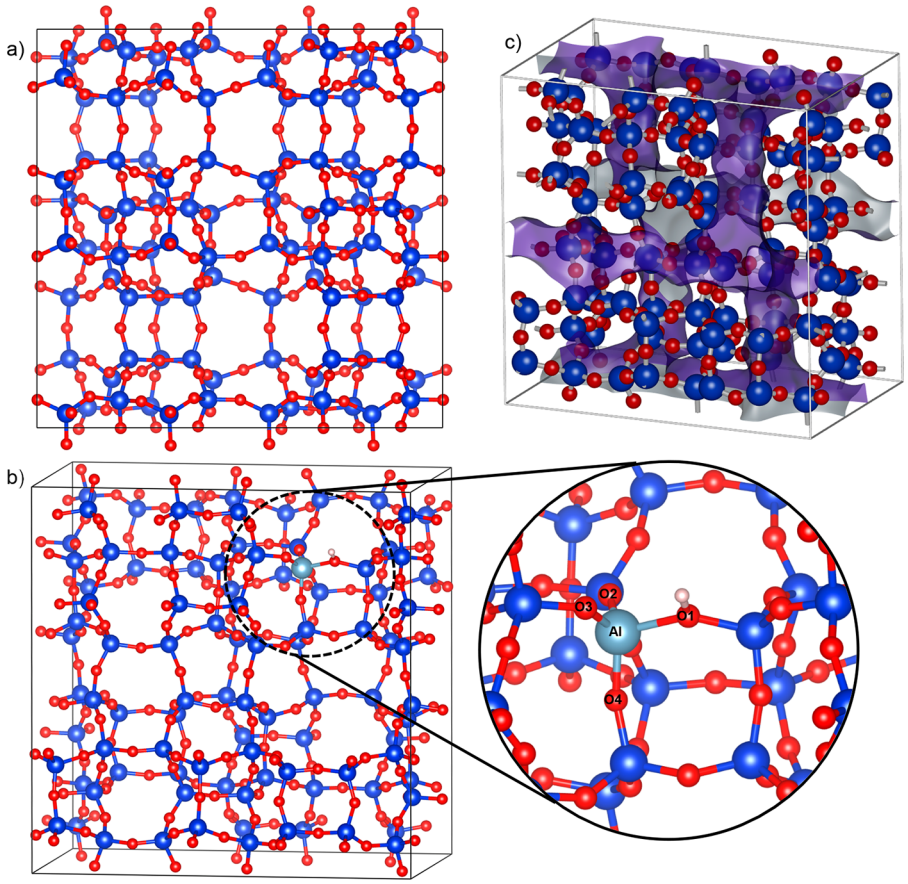

Figure 2. Graphical representations of (a) 2-d projection of the MFI unit cell normal to the **c**-vector, (b) framework aluminum at the T9 position and surrounding oxygen atoms, with the acidic proton located on the O1 oxygen, and (c) internal pore structure of intersecting straight and sinusoidal channels projected as an opaque isosurface within the framework.

A number of studies have reported reaction-specific adsorption energies of monomers and corresponding dimer structures using electronic structure calculations for different heterogeneous catalysts, observing a significant decrease in the differential binding energy of the second adsorbate.[18b,22c,25] However, to the best of our knowledge, a systematic computational examination of monomer/dimer adsorption trends for heterogeneous classes of adsorbates in zeolites has not been explored. Toward this end, we report a systematic study of adsorption thermochemistry for several adsorbate classes in pure-silica and acidic ZSM-5. Specifically, by using periodic electronic structure calculations, we report electronic energies, enthalpies, and free energies of adsorption in HZSM-5 and SiZSM-5 for 40 adsorbates in monomer and dimer configurations. The families of adsorbates considered include paraffins, olefins, amines, carbohydrates, and small non-condensables. The results reported in this work include linear correlations for dimer adsorption energy as a function of monomer for each adsorbate class and zeolite type. Note that only homodimers, i.e., of the same two molecules, were examined here. The correlations reported will improve the accuracy of estimated dimer adsorption energies in ZSM-5 zeolite toward increasing the accuracy of kinetic models.

COMPUTATIONAL METHODS

Fully periodic density functional theory (DFT) calculations were performed with the Vienna ab initio software package (VASP).[26] Plane-wave functions were constructed with the projector augmented wave method (PAW) and energy cutoff of 400 eV.[27] The Brillouin zone was sampled at the Γ-point for all calculations. The generalized gradient approximation (GGA) functional of Perdew, Burke, and Ernzerhof (PBE) was used for all calculations.[27] Dispersion interactions were quantified by including the DFT-D3 empirical correction with Becke and Johnson damping (D3BJ).[28] Geometries were optimized in two steps with the goal of maximizing chemical accuracy with good computational efficiency. Structures were optimized in the first step with a conjugate-gradient algorithm (IBRION = 2) using a wave function convergence criteria keeping energy variations between SCF iterations $<10^{-6}$ eV, and forces were computed with a fast Fourier transform grid of 2× the default energy cutoff (PREC = ACCURATE in VASP). Structures were relaxed until the maximum force on any atom was <0.05 eV/Å. The same structures were reoptimized with a quasi-Newton algorithm (IBRION = 1), with wave functions converged to $<10^{-6}$ eV and maximum force on any atom to <0.01 eV/Å.

The MFI (ZSM-5) framework structure was obtained from the database of the International Zeolite Association (IZA),[6] with unit cell parameters a = 20.090 Å, b = 19.738 Å, c = 13.142 Å, and $a = b = c = 90.0°$. A unit cell optimization with an energy cutoff of 800 eV was performed allowing for the relaxation of atomic positions, unit cell shape, and volume (ISIF = 3), resulting in minor increases of the unit cell parameters a = 20.4431, b = 20.1759, and c = 13.5812. There are 12 unique tetrahedral positions available for Al substitution

https://doi.org/10.1021/acs.jpcb.1c02929
J. Phys. Chem. B 2021, 125, 7199−7212

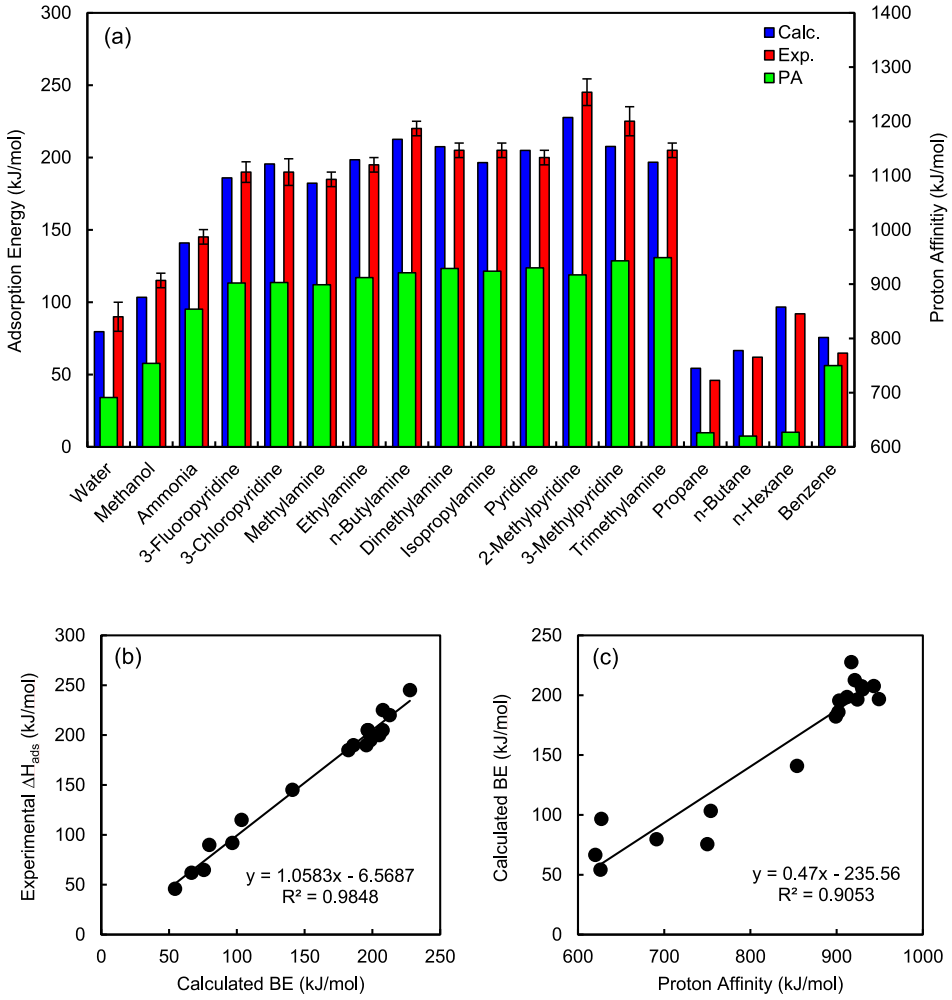

Figure 3. Calculated adsorption energies (ΔE_{ZPE}) and NIST proton affinities (PA) of selected monomer adsorbates in HZSM-5 along with corresponding experimental values from various literature sources.[12a,b,13a,b,14,34] The data are reported (in kJ/mol) as absolute values of adsorption energy in (a) bar graph format, (b) parity plot of experimental versus calculated values, and (c) scatter plot of calculated BE as a function of adsorbate proton affinity.

in the MFI framework, and a number of studies have been performed to identify the most stable and catalytically relevant positions.[16,29] The general consensus is that the relative stabilities of the 12 unique tetrahedra (all containing four possible proton locations) are energetically similar, according to electronic structure calculations.[16] The BA site protons are known to "hop" between the oxygen atoms of the AlO_4^- tetrahedron in ZSM-5 through weakly activated transitions,[30] which can occur independently (E_a = 101 kJ/mol) or facilitated by external OH functionalities such as H_2O (E_a = 29 kJ/mol).[30b] Relative energies of the four possible BA sites were assessed and shown to vary by a maximum of 11.9 kJ/mol, choosing a configuration in a low-lying ground state (Figure 2).

The T9 position is located at an intersection of straight and sinusoidal channels (Figure 2) and was chosen to be substituted by the Al atom (corresponding to Si/Al = 95), allowing adsorbates access to the larger void environment at this intersection. We acknowledge that the T12 site is a commonly used crystallographic position in MFI calculations; however, other studies[29a] have proposed alternate tetrahedral positions that are more energetically favorable for heteroatom substitution relative to the conventionally used T12 models,[16] namely T7 and T9.[29a] It has also been suggested that different tetrahedral positions of the MFI framework can be likely candidates for selective formation of BA site pairs with neighboring tetrahedral positions,[31] while adhering to Loewenstein's rule.[32] Adsorption behavior of an isolated BA site at the T9 position will provide valuable background information for future adsorption studies involving BA site pairs.

Several test calculations were performed to compare the adsorption data at the chosen (T9) tetrahedral position to those at the T12 site to ensure the validity of the reported values. The binding energies for N_2, ethene, and H_2O were calculated at the T12 site, with the most stable position of the acidic proton selected for these calculations. The calculated monomer BEs were generally found to be slightly more exergonic relative to the T9, with ΔBE_{T12-T9} of −7.4, −4.3, and −0.7 kJ/mol for N_2, ethene, and H_2O monomers, respectively. The deviations in dimer BEs were of similar order, with the calculated ΔBE_{T12-T9} of +0.5, −4.8, and −7.0 kJ/mol for N_2, ethene, and H_2O dimers, respectively.

Binding energies of adsorbates in the SiZSM-5 and HZSM-5 systems will be calculated in reference to adsorbates and zeolite sites at infinite separation, according to eq 1

$$BE = E_{complex} - E_{zeolite} - nE_{adsorbate} \quad (1)$$

https://doi.org/10.1021/acs.jpcb.1c02929
J. Phys. Chem. B 2021, 125, 7199−7212

Table 1. Adsorption Thermochemistry Values Calculated for Adsorbate Monomer and Dimer States in HZSM-5[a]

	monomer				dimer			
species	ΔE_0	ΔE_{ZPE}	ΔH	ΔG	ΔE_0	ΔE_{ZPE}	ΔH	ΔG
CO	−33.3	−25.5	−41.3	24.9	−54.2	−43.6	−89.9	39.5
N_2	−34.2	−26.0	−39.2	27.6	−63.6	−51.8	−94.1	30.0
H_2	−19.4	−8.9	−23.4	22.8	−38.8	−21.0	−58.9	26.1
He	−48.1	−43.3	−54.2	−11.0	−51.2	−45.1	−67.3	−6.2
Ne	−51.2	−46.4	−57.3	−8.1	−56.9	−50.8	−73.1	−6.0
Ar	−63.9	−59.1	−69.9	−18.3	−79.7	−71.1	−98.8	−19.5
water	−89.8	−79.7	−94.7	−30.3	−158.6	−141.6	−177.4	−79.9
methanol	−111.8	−103.4	−119.3	−36.5	−201.4	−186.7	−234.5	−94.5
ethanol	−121.6	−114.0	−135.1	−38.7	−233.3	−216.3	−276.7	−110.3
ammonia	−156.1	−141.0	−155.9	−90.8	−256.9	−230.2	−266.1	−167.8
2-fluoropyridine	−183.3	−169.6	−197.7	−86.9	−276.3	−257.8	−337.4	−131.3
3-fluoropyridine	−201.4	−186.0	−214.3	−103.1	−303.2	−282.9	−363.6	−154.4
3-chloropyridine	−211.2	−195.6	−225.5	−109.4	−320.0	−299.2	−384.1	−165.6
methylamine	−199.4	−182.3	−201.1	−117.3	−299.5	−274.7	−326.5	−184.9
ethylamine	−216.7	−198.5	−222.6	−125.3	−336.2	−311.4	−377.6	−204.6
n-butylamine	−231.7	−212.7	−250.3	−121.6	−390.1	−365.4	−466.1	−217.3
dimethylamine	−225.7	−207.5	−231.9	−134.0	−309.1	−284.8	−353.3	−175.4
isopropylamine	−216.9	−196.5	−226.6	−116.4	−361.8	−337.7	−421.0	−213.4
pyridine	−220.9	−204.9	−229.3	−127.0	−322.6	−301.7	−372.8	−181.1
2-methylpyridine	−244.9	−227.7	−261.1	−138.5	−352.1	−329.4	−423.0	−185.1
3-methylpyridine	−224.6	−207.7	−241.1	−118.5	−365.8	−345.5	−438.4	−203.9
trimethylamine	−218.0	−196.7	−226.8	−116.7	−292.4	−263.9	−346.6	−143.8
methane	−36.7	−28.1	−45.7	36.2	−61.0	−48.2	−101.1	51.4
ethane	−55.6	−47.1	−68.0	15.2	−93.9	−82.5	−145.8	24.6
propane	−62.6	−54.3	−81.4	21.4	−118.5	−106.6	−184.6	20.3
n-butane	−75.1	−66.6	−100.3	18.1	−150.3	−138.7	−233.2	5.3
i-butane	−81.5	−70.7	−103.0	10.9	−143.0	−128.6	−219.4	2.0
n-hexane	−105.9	−96.7	−143.9	6.2	−202.0	−188.0	−316.0	−10.1
2-methylpentane	−93.5	−82.1	−128.3	17.3	−198.8	−182.9	−308.9	−9.6
3-methylpentane	−78.9	−67.1	−113.3	31.9	−163.4	−145.3	−270.2	21.4
2,3-dimethylbutane	−85.3	−72.4	−118.5	25.5	−153.6	−133.3	−256.4	26.8
2,2-dimethylbutane	−51.9	−37.5	−82.8	57.9	−130.9	−111.8	−237.6	59.0
ethene	−67.8	−59.1	−77.2	2.3	−107.4	−94.1	−147.7	0.3
propene	−91.3	−82.0	−106.3	−7.5	−152.9	−138.7	−207.8	−24.4
1-butene	−104.6	−94.6	−124.7	−12.4	−187.3	−172.2	−256.6	−40.1
c-2-butene	−106.1	−95.9	−127.9	−9.4	−191.6	−176.3	−265.2	−35.7
t-2-butene	−113.3	−102.9	−135.1	−17.3	−206.0	−190.9	−280.4	−50.6
i-butene	−113.3	−104.6	−135.2	−22.2	−170.1	−154.3	−238.7	−27.5
1-hexene	−138.5	−127.7	−171.3	−27.5	−235.7	−220.7	−340.9	−45.6
E-2-hexene	−144.1	−133.5	−178.9	−30.8	−263.5	−247.6	−371.3	−67.3
Z-2-hexene	−130.3	−120.0	−164.8	−17.6	−221.2	−203.6	−325.1	−28.5
E-3-hexene	−148.5	−138.4	−183.2	−37.0	−250.1	−231.8	−353.2	−56.8
Z-3-hexene	−128.1	−115.8	−159.6	−15.6	−234.4	−217.2	−338.4	−42.2
benzene	−86.3	−75.6	−115.9	51.3	−164.2	−150.6	−239.8	19.2

[a]Enthalpies (ΔH) and free energies (ΔG) of adsorption were calculated at 298.15 K and 1 atm. Olefin adsorption is reported as π-complex binding energies (physisorption). Values are reported in kJ/mol.

where $E_{complex}$ corresponds to the energy of the adsorbate complex, $E_{zeolite}$ to the energy of the empty zeolite framework, and $E_{adsorbate}$ to the gas-phase energy of the adsorbate. Vibrational frequency calculations were used to approximate zero-point vibrational energies (ZPE), vibrational enthalpies (H), and free energies (G) by using a fixed displacement method ($n = 2$) for all gas-phase and adsorbed species. Framework Si and O atoms not bound to the Al atom were fixed within the zeolite framework during frequency calculations in HZSM-5, while all framework atoms were fixed in SiZSM-5 systems. System enthalpies and free energies were approximated by using statistical thermodynamics, according to eqs 2 and 3

$$H = E_0 + E_{ZPE} + H_{vib} + H_{trans} + H_{rot} \quad (2)$$

$$G = E_0 + E_{ZPE} + G_{vib} + G_{trans} + G_{rot} \quad (3)$$

where E_0 is the total electronic energy of the system, E_{ZPE} is the zero-point vibrational energy, H/G_{vib} is vibrational contribution to state functions, H/G_{trans} denotes the translational contribution to state functions, and H/G_{rot} is the rotational contribution to state functions. All motions for guest molecules within the MFI framework were considered vibrations, such

https://doi.org/10.1021/acs.jpcb.1c02929
J. Phys. Chem. B 2021, 125, 7199−7212

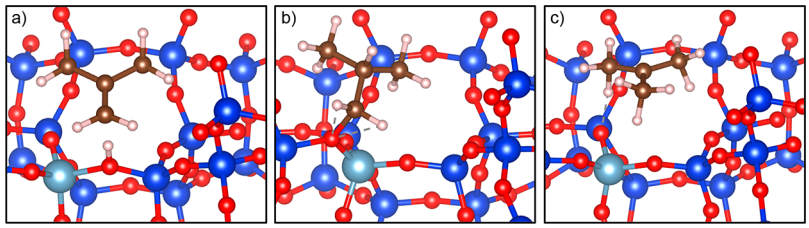

Figure 4. Graphical representation of monomer states of isobutene adsorbed in the HZSM-5 framework. The π-complex (a), alkoxide (b), and carbenium ion (c) configuerations are shown.

that translations and rotations were frustrated, with H and G values assumed to be zero for non-gas-phase species. Low-frequency vibrational modes below 60 cm^{-1} were replaced by 60 cm^{-1}, toward eliminating disproportionate contributions toward estimated state functions, as reported by Di Iorio et al.[4a]

RESULTS AND DISCUSSION

1. Adsorption of Different Complexes in HZSM-5. The adsorption behavior of different adsorbate classes including paraffins, olefins, amines, carbohydrates, water, and non-condensible gases in the HZSM-5 model system was assessed. Geometry optimization calculations were performed to obtain stable ground states, resulting in spatial configurations that maximize adsorbate interactions with the BA proton, while minimizing steric constraints imposed by the pore walls. Several different starting configurations were considered for the adsorbates to ensure sufficient energetic minima on the potential energy landscape were sampled. However, it is possible that more stable ground states may exist for the adsorbates considered.

To ensure the chemical accuracy of all calculations, experimental enthalpies of adsorption were compared to DFT-calculated monomer binding energies for several adsorbate classes. The ZPE-corrected energies of adsorption showed best agreement with experiments (Figure 3), with good agreement observed for most adsorbates (RMSD = 2.17). Amines were found to interact the strongest with the BA sites, followed by carbohydrates, water, olefins, and paraffins. Largest deviations from experimental measurements were observed for bulky amine molecules such as 2-methylpyridine (18 kJ/mol) and 3-methylpyridine (17 kJ/mol). The calculated adsorption energies, enthalpies, and free energies of the monomer and dimer states for all adsorbates are reported in Table 1. Qualitative agreement in trends of ΔE_{ZPE} with PA values obtained from NIST[33] was observed for all adsorbates reported in Figure 3a. Quantitative agreement between experimental enthalpies of adsorption and calculated values are demonstrated in Figure 3b in the form of a parity plot, with a strong linear correlation observed. Additionally, calculated BE values were found to correlate with the adsorbate PA (Figure 3c), although the trends are subject to point scatter.

A sample graphical representation of adsorbed isobutene ground states in the monomer configurations is shown in Figure 4. The physisorbed π-complex in the monomer state is shown in panel a, with corresponding ΔE_{ZPE} of −104.6 kJ/mol. The chemisorbed alkoxide complex in the monomer state is shown in panel b, with corresponding ΔE_{ZPE} of −117.0 kJ/mol. Finally, the tertiary carbenium ion interacting with the framework conjugate base anion in the monomer state is shown in panel c, with a corresponding ΔE_{ZPE} of −82.9 kJ/mol. It should be noted that a proportional increase of monomer BE was not observed for the dimer species, with the π-complexation, chemisorption, and carbenium ion binding energies corresponding to −154.3, −138.5, and −151.9 kJ/mol, respectively. A detailed discussion of energetics in physisorption and chemisorption of olefins can be found in section 3 of the Results and Discussion (*vide infra*).

As stated previously, some adsorbates can spontaneously deprotonate a BA site upon adsorption and create an acid−base pair. For example, the adsorption of NH_3 (Figure 5)

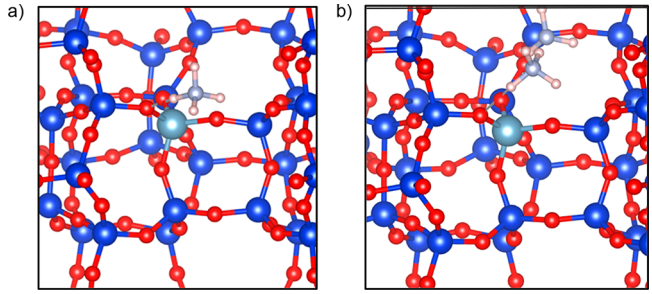

Figure 5. Graphical representation of adsorbed NH_3 molecules in (a) monomer and (b) dimer states. A cation−anion pair is formed in both cases following a spontaneous deprotonation of the BA site.

results in a spontaneous deprotonation of the BA site, forming an acid−conjugate base complex for both monomer and dimer configurations. Based on the calculation results, NH_3 is the least basic (lowest PA) adsorbate in our data set that spontaneously deprotonates the BA site. This suggests that there may exist a critical PA value for which any adsorbate will deprotonate an acid site—based on our results, adsorbates characterized by PA in the range of −750 to −850 kJ/mol are likely candidates. One should note that additional considerations such as pore topology and adsorbate structure may affect the extent of deprotonation, limiting our analysis to the MFI framework and the adsorbates considered.

Dimer adsorption energies for most adsorbates considered followed the behavior of isobutene shown in Figure 4, with the total BE of dimers in HZSM-5 being a fraction of the doubling of monomer BE. The adsorption energies of dimer versus monomer states are plotted in Figure 6, with a linear trend observed between the two sets of calculated values. A linear correlation was observed, with a slope of 1.46 and a y-intercept value of −21.3; the slope implies a linear dependence of dimer BE on that of monomer, while the y-intercept value can be attributed to (adsorbate) intermolecular interactions in the dimer state, in addition to adsorbate−zeolite interactions. It can be seen that the linear fit does not intersect the origin, largely due to point scatter among the different adsorbate classes. Interestingly, if one were to exclude amines as a class, a

https://doi.org/10.1021/acs.jpcb.1c02929
J. Phys. Chem. B 2021, 125, 7199−7212

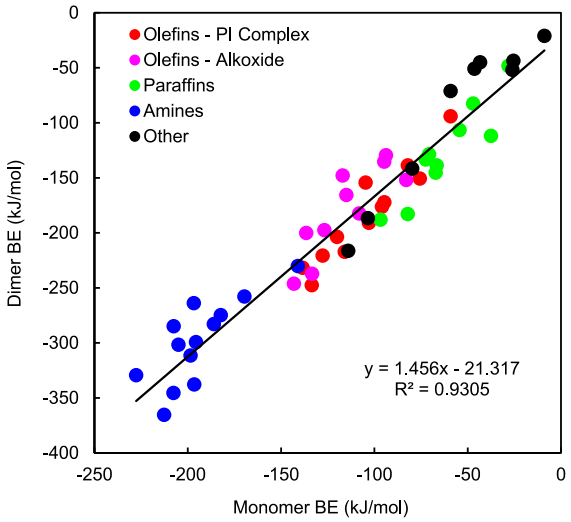

Figure 6. Calculated values of ΔE_{ZPE} of dimer versus monomer configurations in HZSM-5 with the adsorbate classes of paraffins, olefins (π-complex and alkoxide), amines, and all others represented by green, red, magenta, blue, and black markers, respectively. Values are reported in kJ/mol.

linear fit would result in a significantly decreased y-intercept value.

Amines were found to bind the strongest, followed by olefins and paraffins. The distribution of calculated BEs for the remaining adsorbates was found to vary significantly due to the heterogeneity of adsorbate types in this class. These observations are consistent with calorimetry and gravimetry experiments for different acidic zeolites, in which heats of adsorption decrease significantly with increasing adsorbate loadings in HZSM-5.[20−22,24,25,28] It should be noted that correlations specific to each adsorbate class would likely be different due to varying physicochemical properties of each class, such as molecular identity, size, and shape. A detailed discussion of these trends can be found in section 4 of the Results and Discussion (*vide infra*).

It should be noted that a number of adsorbates exhibited positive values of ΔG_{ads} in both monomer and dimer states for adsorption events in HZSM-5 and SiZSM-5, suggesting that these adsorption events may be unfavorable. However, it has been observed by previous authors that the harmonic oscillator approximation for the normal vibrational modes of adsorbates and zeolite framework atoms may result in poor estimates of the entropic losses during these events and deviations of ΔG_{ads} from experimental values at finite temperatures.[35] Therefore, ΔE_{ZPE} will be used as the computational measure of adsorption energies for the duration of this work based on previous studies and benchmark calculations reported in Figure 3.

2. Adsorption of Different Complexes in SiZSM-5. In addition to modeling the acidic zeolite system, a pure silica framework (SiZSM-5) was used to probe the adsorption behavior in silicalite for the adsorbate set considered in HZSM-5 (*vide supra*). In the absence of a BA site, adsorption events are driven exclusively by (weak) adsorbate−framework and adsorbate−adsorbate (in the case of dimers) interactions, namely dispersion and van der Waals interactions. In the absence of acidic functionalities, one would expect fully proportional, i.e., doubling of, monomer adsorption energies for dimer states. The presence of two adsorbates in the SiZSM-5 unit cell in the case of dimer adsorption still corresponds to low experimental loadings. Furthermore, molecular adsorption experiments in silicalite have shown no variation in measured heats of adsorption for a wide range of adsorbate loadings.[8,9]

The adsorption energies of dimer versus monomer states in SiZSM-5 are plotted in Figure 7, with a linear trend also

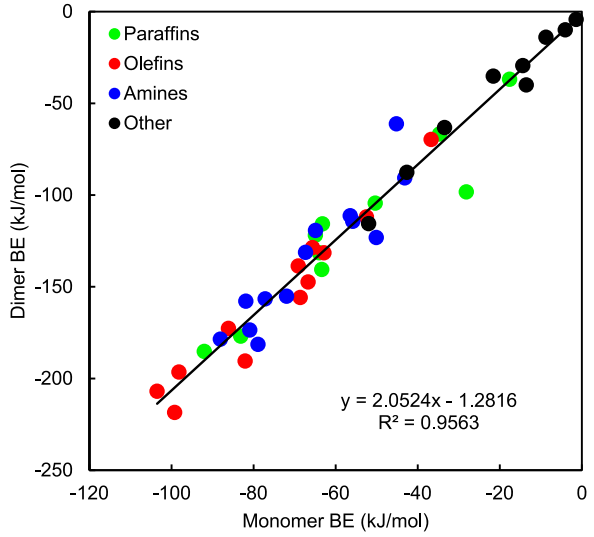

Figure 7. Calculated values of ΔE_{ZPE} of dimer versus monomer configurations in SiZSM-5 with the adsorbate classes of paraffins, olefins, amines, and all others represented by green, red, blue, and black markers, respectively. Values are reported in kJ/mol.

observed between the two sets of calculated values. Long-chain olefins and paraffins were found to bind the strongest, with amines and the remaining adsorbates spanning a wide range of BE values. The calculated adsorption energies, enthalpies, and free energies of the monomer and dimer states for all adsorbates in SiZSM-5 are reported in Table 2. As evidenced by the slope of a fitted line, the dimer binding energies are nearly double of the monomer BEs, in agreement with silicalite adsorption experiments.[8,9] Additional discussion of adsorbate-specific trends can be found in sections 3 and 4 of the Results and Discussion (*vide infra*).

3. Olefin Adsorption. As stated previously, adsorption of olefins can occur in different modes, including physisorbed π-complexes, chemisorbed alkoxides, and carbenium ions. The relative populations of these states at operating conditions are a function of a number of physicochemical properties of the adsorbate and sorbent, including adsorbate size and degree of branching, as well as the local environment around the BA site.

The distinction between physisorption and chemisorption is significant, with physisorption referring to a state in which the π-electrons of the C═C double bond interact with the H acid proton as well as any weak interactions with the zeolite walls. Chemisorption refers to a state in which the acidic proton is transferred to the adsorbate and a covalent C−O bond is formed with the zeolite framework,[36] as shown in Figure 1. However, for branched alkenes, such as isobutene, the state of the adsorbates has been under further scrutiny. Species capable of stable tertiary carbocations have been suggested to form tertiary carbenium ions in zeolite pores; the protonated olefin species has a positive charge that keeps it complexed with the negatively charged framework. The relative stabilities of the *tert*-butoxy alkoxide and the *tert*-butylcarbenium ion have been

https://doi.org/10.1021/acs.jpcb.1c02929
J. Phys. Chem. B 2021, 125, 7199−7212

Table 2. Adsorption Thermochemistry Values Calculated for Adsorbate Monomer and Dimer States in SiZSM-5[a]

	monomer				dimer			
species	ΔE_0	ΔE_{ZPE}	ΔH	ΔG	ΔE_0	ΔE_{ZPE}	ΔH	ΔG
CO	−21.6	−21.6	−31.5	24.7	−35.1	−35.2	−45.1	11.1
N_2	−13.5	−13.5	−21.0	36.1	−40.0	−40.0	−47.4	9.6
H_2	−9.4	−8.8	−18.7	20.1	−15.2	−14.0	−23.9	14.9
He	−1.4	−1.4	−8.8	28.7	−4.3	−4.3	−11.7	25.9
Ne	−4.0	−4.0	−11.5	32.1	−9.9	−9.9	−17.4	26.2
Ar	−14.4	−14.4	−21.8	24.3	−29.5	−29.5	−36.9	9.2
water	−33.2	−33.5	−43.4	12.8	−74.3	−63.2	−85.0	−9.5
methanol	−42.9	−42.6	−52.7	20.2	−93.6	−87.6	−122.2	3.2
ethanol	−52.9	−52.0	−67.3	19.3	−122.3	−115.6	−163.3	−9.8
ammonia	−45.4	−45.2	−55.3	2.1	−68.5	−61.2	−89.4	2.7
2-fluoropyridine	−68.0	−67.3	−89.2	11.0	−135.8	−131.3	−195.8	−7.5
3-fluoropyridine	−78.3	−77.2	−99.3	1.3	−161.1	−156.6	−221.6	−33.2
3-chloropyridine	−89.6	−88.1	−112.0	−6.4	−183.5	−178.6	−247.8	−49.9
methylamine	−43.3	−43.1	−56.4	17.8	−95.9	−90.7	−130.5	0.0
ethylamine	−56.9	−56.5	−75.1	13.0	−117.3	−111.3	−164.5	−6.4
n-butylamine	−81.7	−80.9	−113.3	7.2	−180.0	−173.6	−261.5	−26.7
dimethylamine	−65.5	−64.9	−83.3	4.4	−123.2	−119.3	−174.6	−8.5
isopropylamine	−52.9	−50.1	−74.6	26.0	−130.5	−123.2	−192.5	−4.7
pyridine	−83.0	−81.9	−100.0	−8.4	−162.4	−157.9	−212.8	−43.7
2-methylpyridine	−80.6	−78.9	−106.2	6.0	−187.1	−181.4	−259.3	−41.8
3-methylpyridine	−73.9	−72.0	−99.3	13.2	−160.4	−155.1	−232.9	−16.8
trimethylamine	−57.6	−55.8	−79.6	19.5	−118.8	−114.3	−183.9	8.9
methane	−17.6	−17.6	−27.7	41.5	−40.0	−36.9	−71.3	54.6
ethane	−34.6	−34.7	−48.2	22.4	−69.5	−66.8	−110.1	28.7
propane	−50.8	−50.4	−69.3	19.4	−108.0	−104.4	−162.1	10.4
n-butane	−64.6	−64.0	−89.9	15.2	−135.8	−131.5	−205.7	−0.1
i-butane	−65.0	−63.2	−88.6	13.7	−122.8	−115.7	−187.1	3.1
n-hexane	−93.6	−92.0	−131.7	5.7	−191.6	−185.3	−292.6	−20.4
2-methylpentane	−85.1	−83.1	−122.5	12.1	−183.5	−176.9	−284.9	−12.8
3-methylpentane	−68.1	−63.4	−102.0	30.4	−151.8	−140.6	−245.3	13.5
2,3-dimethylbutane	−70.2	−64.9	−103.3	26.9	−135.2	−121.9	−225.3	26.2
2,2-dimethylbutane	−33.7	−28.1	−66.7	62.6	−111.1	−98.3	−202.4	50.6
ethene	−36.7	−36.7	−47.9	19.9	−72.3	−69.7	−107.7	24.8
propene	−53.8	−52.5	−69.9	17.2	−116.6	−111.9	−164.4	0.0
1-butene	−67.9	−66.7	−90.2	11.3	−152.3	−147.4	−215.4	−18.3
c-2-butene	−71.1	−69.1	−94.3	12.5	−144.7	−138.7	−210.5	−3.2
t-2-butene	−70.7	−68.6	−94.2	12.3	−161.9	−155.8	−227.8	−23.2
i-butene	−66.8	−65.6	−89.5	11.9	−136.2	−128.7	−195.5	−10.0
1-hexene	−100.1	−98.2	−135.5	−1.3	−202.4	−196.5	−299.5	−27.5
E-2-hexene	−101.4	−99.2	−138.2	−0.3	−225.5	−218.5	−324.6	−46.1
Z-2-hexene	−88.1	−86.1	−124.3	12.3	−181.5	−172.7	−276.5	−5.3
E-3-hexene	−105.2	−103.5	−141.9	−5.8	−215.9	−207.0	−310.6	−40.4
Z-3-hexene	−85.6	−82.1	−119.5	14.2	−197.7	−190.5	−294.3	−23.4
benzene	−64.6	−62.8	−95.8	58.8	−135.8	−131.5	−201.8	29.1

[a]Enthalpies (ΔH) and free energies (ΔG) of adsorption were calculated at 298.15 K and 1 atm. Values are reported in kJ/mol.

mixed in the literature, depending on the zeolite pore size and topology as well as computational methods used.[37]

Table 3 reports the energetics of physisorption and chemisorption of various alkenes in HZSM-5, with their energetic difference reported as protonation energy (ΔE_{prot}). The formation of alkoxide states was found to be exergonic relative to physisorbed sates for small linear olefins. Interestingly, nonlinear C4 and C6 olefins exhibited significantly lower protonation energies, with several species being less stable in the chemisorbed state. This is in agreement with findings by Rozanska et al.[37a] and Nguyen et al.,[24b] which found in small pore zeolites, such as H-CHA and H-ZSM-22, the confined environments induce steric constraints that destabilize the bulky alkoxide states. These findings further suggest that highly branched structures may have different ground states relative to linear counterparts.

4. Adsorption Trends for Monomer and Dimer Complexes. A number of trends were observed for the calculated monomer and dimer adsorption energies in acidic and pure-silica zeolite systems, with generally strong linear correlations. The data reported in this section will be based on zero-point corrected binding energies (ΔE_{ZPE}), with corresponding correlations based on other thermochemical values, ΔH and ΔG, reported in the Supporting Information.

Upon closer examination of Figure 6, a certain "curvature" in the data set was observed, suggesting that among the different

https://doi.org/10.1021/acs.jpcb.1c02929
J. Phys. Chem. B 2021, 125, 7199−7212

Table 3. Energies of Physisorption (ΔE_{phys}), Chemisorption (ΔE_{chem}), and Protonation (ΔE_{prot}) of Various Alkenes in HZSM-5, Reported in kJ/mol

species	π-complex to alkoxide	ΔE_{phys}	ΔE_{chem}	ΔE_{prot}
1-alkenes	ethene to ethoxy	−59.1	−93.8	−34.6
	propene to 2-propoxy	−82.0	−115.0	−32.9
	1-butene to 2-butoxy	−94.6	−108.1	−13.4
	1-hexene to 2-hexoxy	−127.7	−143.1	−15.4
2-alkenes	*cis*-2-butene to 2-butoxy	−95.9	−94.7	1.2
	trans-2-butene to 2-butoxy	−102.9	−100.0	3.0
	E-2-hexene to 2-hexoxy	−133.5	−143.1	−9.6
	Z-2-hexene to 2-hexoxy	−120.0	−136.5	−16.5
3-alkenes	*E*-3-hexene to 3-hexoxy	−138.4	−133.4	5.1
	Z-3-hexene to 3-hexoxy	−115.8	−126.8	−10.9

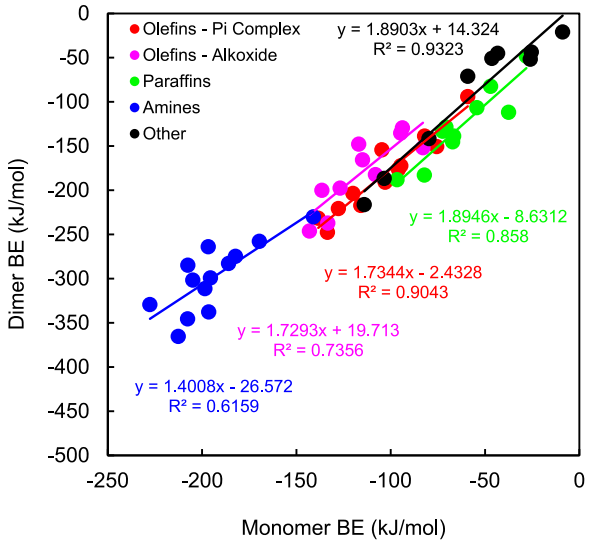

Figure 8. Calculated values of ΔE_{ZPE} of dimer versus monomer configurations in HZSM-5 with the adsorbate classes of paraffins, olefins, amines, and all others represented by green, red, magenta, blue, and black markers, respectively. Linear correlations for each adsorbate class are reported in accordance with the data series color scheme. Values are reported in kJ/mol.

classes of adsorbates there may be individual unique correlations. Figures 8 and 9 report specific linear correlations for each of the adsorbate classes in the HZSM-5 and SiZSM-5 systems, respectively. Significant variability in trend line slopes was observed for the acidic zeolite systems, while little to no variability was observed among adsorbate classes in silicalite systems with proportional increases in monomer BEs observed.

The individual correlations reported in Figure 8 were applied as linear scaling relations to better estimate dimer BEs across all adsorbate classes. The scaling relations to estimate adsorbate class-specific BE values are shown in eqs 4−8.

$$BE_{dimer,amine} = 1.40 \times BE_{monomer,amine} - 26.6 \quad (4)$$

$$BE_{dimer,olefin,phys} = 1.73 \times BE_{monomer,olefin,phys} - 2.4 \quad (5)$$

$$BE_{dimer,olefin,chem} = 1.73 \times BE_{monomer,olefin,phys} + 19.7 \quad (6)$$

$$BE_{dimer,paraffin} = 1.89 \times BE_{monomer,paraffin} - 8.6 \quad (7)$$

$$BE_{dimer,other} = 1.89 \times BE_{monomer,other} + 14.3 \quad (8)$$

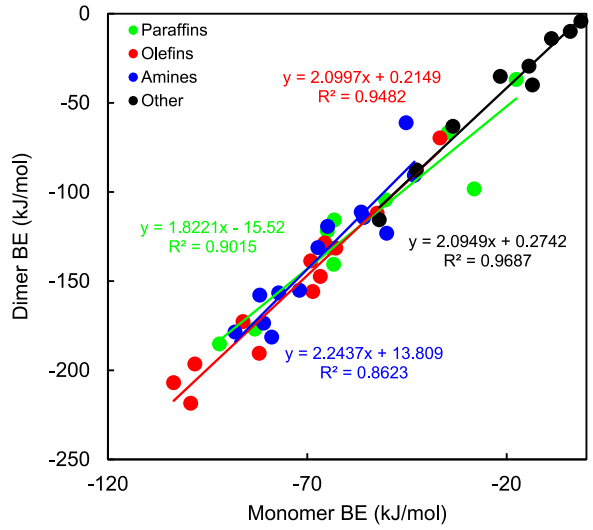

Figure 9. Calculated values of ΔE_{ZPE} of dimer versus monomer configurations in SiZSM-5 with the adsorbate classes of paraffins, olefins, amines, and all others represented by green, red, blue, and black markers, respectively. Linear correlations for each adsorbate class are reported in accordance with the data series color scheme. Values are reported in kJ/mol.

where BE_{dimer} and $BE_{monomer}$ correspond to adsorption energies for the dimer and monomer states in HZSM-5, respectively. The correlations contained in eqs 4−8 provide a practical deliverable of this work, which other researchers can adopt for implementation of screening studies or kinetic modeling. To illustrate how well these correlations would predict the adsorption of dimers in the classes of molecules examined here, but not explicitly calculated by using DFT, the correlations in eqs 4−8 were used to predict the dimer BEs from the monomer BE values calculated by using DFT. The results were compared to the actual dimer binding energies calculated by using DFT in the form of a parity plot, shown in Figure 10. Good agreement between model predicted and DFT-calculated dimer BEs was observed for all adsorbate

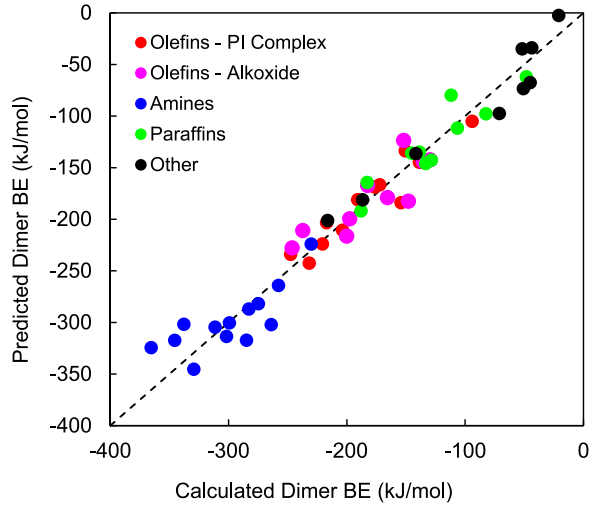

Figure 10. Parity plot of model-predicted and DFT-calculated dimer adsorption energies in HZSM-5. The adsorbate classes of paraffins, olefins, amines, and all others represented by green, red, magenta, blue, and black markers, respectively. Values are reported in kJ/mol.

https://doi.org/10.1021/acs.jpcb.1c02929
J. Phys. Chem. B 2021, 125, 7199−7212

classes, as shown in Figure 10. This reveals that if the binding energy of the monomer alone is available, the dimer binding energy can be reasonably estimated without having to perform costly DFT calculations that typically more than double the resource requirements, depending on the size of the adsorbate considered.

The largest point scatter was observed for amines, followed by (chemisorbed) olefins, paraffins, (physisorbed) olefins, and small adsorbates, with corresponding RMSD values of 6.37, 6.28, 4.80, 3.78, and 5.80, respectively. These trends can be rationalized by the large degree of heterogeneity in terms of molecular structure among the amines, resulting in significant scatter due to steric hindrance imposed on bulkier adsorbates by the local pore environment around the BA site. Overall, these correlations can be a powerful tool in estimating dimer formation energies using as input only monomer data for a range of adsorbate classes in acidic ZSM-5 zeolites.

Using identical methodology, the individual correlations presented in Figure 9 were used to construct scaling relations for prediction of dimer adsorption energies in SiZSM-5 for the four adsorbate subclasses and reported in eqs 9−12. As stated previously, in the absence of BA site functionality, the dimer adsorption energies were found to increase proportionately relative to the monomer values, which is evidenced by the scaling factors reported in eqs 9−12.

$$BE_{dimer,amine} = 2.24 \times BE_{monomer,amine} + 13.8 \quad (9)$$

$$BE_{dimer,olefin} = 2.10 \times BE_{monomer,olefin,phys} + 0.2 \quad (10)$$

$$BE_{dimer,paraffin} = 1.82 \times BE_{monomer,paraffin} - 15.5 \quad (11)$$

$$BE_{dimer,other} = 2.09 \times BE_{monomer,other} + 0.3 \quad (12)$$

The results were compared to the actual dimer binding energies calculated by using DFT in the form of a parity plot, shown in Figure 11.

In addition, we take a closer look at two adsorbate classes, olefins and paraffins, and their adsorption behavior as monomer and dimer states as a function of carbon number

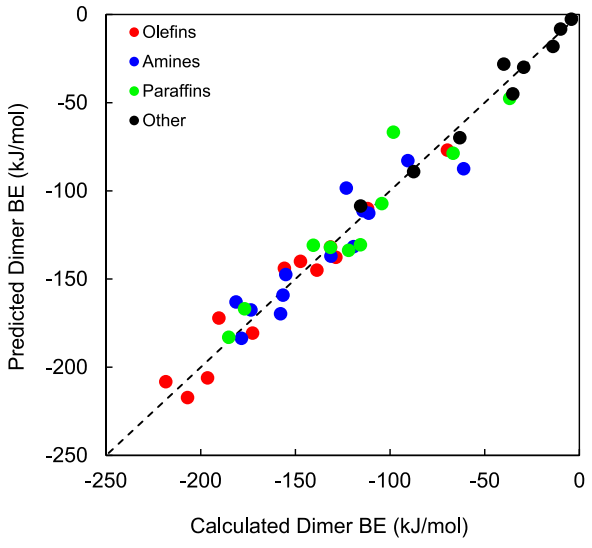

Figure 11. Parity plot of model-predicted and DFT-calculated dimer adsorption energies in SiZSM-5. The adsorbate classes of paraffins, olefins, amines, and all others are represented by green, red, blue, and black markers, respectively. Values are reported in kJ/mol.

(CN) in the two zeolite systems. Specifically, additional scaling relations were developed for C2−C6 linear paraffin and α-olefin species in the HZSM-5 and SiZSM-5 systems.

The DFT-calculated adsorption energies of monomer and dimer complexes of linear C2−C6 alkanes and alkenes in HZSM-5 are reported in Figure 12. Individual linear fits were

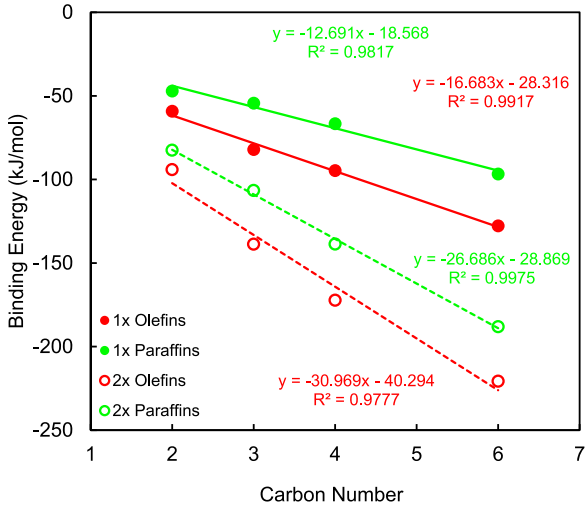

Figure 12. Calculated physisorption energies (ΔE_{ZPE}) of linear paraffin (green) and linear α-olefin (red) species in monomer and dimer configurations in HZSM-5 as a function of carbon number. Note that the data is a subset of that shown in Figures 5 and 7 but is plotted here as a function of CN to provide predictive correlations that would not require any additional DFT calculations. Values are reported in kJ/mol.

added to each set of data points, with good correlation coefficients observed in all cases. Alkenes bind more strongly than alkanes in all cases for monomer and dimer complexes and were found to exhibit stronger dependence on the adsorbate carbon number. The slopes for the adsorption of dimers roughly double that of the corresponding monomer values for both paraffins and olefins. The linear correlations reported in Figure 12 are concisely summarized in eqs 13−16 for easy reference.

$$BE_{monomer,paraffin} = -12.7 \times CN - 18.7 \quad (13)$$

$$BE_{dimer,paraffin} = -26.7 \times CN - 28.9 \quad (14)$$

$$BE_{monomer,olefin} = -16.7 \times CN - 28.3 \quad (15)$$

$$BE_{dimer,olefin} = -31.0 \times CN - 40.3 \quad (16)$$

De Moor et al.[24a] have previously reported correlations for estimating adsorption energies of C2−C8 alkanes in HZSM-5 using electronic structure calculations. The authors also reported linear correlations for BE estimates, in which the y-intersect corresponded to the constant energetic contribution independent of adsorbate size, while the slope corresponded to the contribution by each additional carbon atom (termed β and α, respectively). Reasonable agreement was observed between values reported by De Moor and co-workers of α = −14.0 and β = −22.0 and those obtained in this study of α = −12.7 and β = −18.9. The present work expands on this previous work by extending the analysis to dimers.

Using the same methodology, Nguyen et al.[24b] developed carbon-number-based correlations of linear (C2−C8) olefin

https://doi.org/10.1021/acs.jpcb.1c02929
J. Phys. Chem. B 2021, 125, 7199−7212

BEs as a function of molecular size for several acidic zeolite frameworks, including HZSM-5. Relatively poor agreement was observed between parameters estimated by Nguyen et al. (α = −8.2, β = −41.0) and those obtained in this work (α = −16.7, β = −29.4). These differences can be attributed to the difference in model systems used and the computational methods applied, with Nguyen and co-workers utilizing a hybrid functional (B3LYP) implemented in a QM/MM embedded cluster scheme. Additionally, adsorbate−zeolite interactions were manually tuned toward greater chemical accuracy based on experimental observations.

In Figure 13, we report DFT-calculated adsorption energies of monomer and dimer complexes of linear C2−C6 paraffins

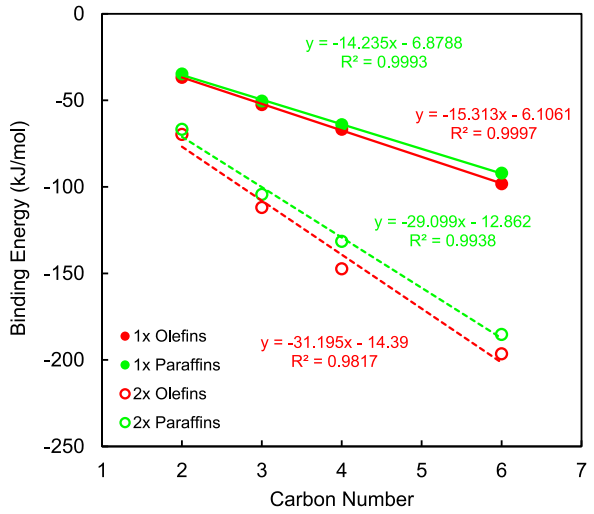

Figure 13. Calculated adsorption energies (ΔE_{ZPE}) of linear paraffin (green) and corresponding α-olefin (red) species in monomer and dimer configurations in SiZSM-5 as a function of carbon number. The data is a subset of that shown in Figures 6 and 8 but is plotted here as a function of CN to provide predictive correlations that would not require any additional DFT calculations. Values are reported in kJ/mol.

and α-olefins in SiZSM-5. BE values for monomer configurations of paraffins and olefins were nearly identical, with slightly stronger adsorption observed for the olefin species. This difference is increased in the case of corresponding olefin dimer BEs, while an almost exact doubling of monomer BEs was observed for all paraffins. Calculated slopes in dimer adsorption also were double those of the corresponding monomer values for both paraffins and olefins, in agreement with the trends observed in HZSM-5. The linear fits reported in Figure 13 are summarized as the linear correlations of monomer and dimer adsorption energies (in kJ/mol) for paraffins and olefins, reported as eqs 17−20.

$$BE_{monomer,paraffin} = -14.2 \times CN - 6.9 \quad (17)$$

$$BE_{dimer,paraffin} = -29.1 \times CN - 12.9 \quad (18)$$

$$BE_{monomer,olefin} = -15.3 \times CN - 6.1 \quad (19)$$

$$BE_{dimer,olefin} = -31.2 \times CN - 14.4 \quad (20)$$

Finally, it has been reported by Studt and co-workers[38] that the dispersion contributions to the BEs of hydrocarbons can correlate with observed BEs and even transition state energies in the case of carbohydrate adsorption and dehydration over HZSM-5. Identical trends were observed in this work, for BEs of monomer and dimer states of olefin and paraffin species, with strong correlations of calculated BE and the dispersion contributions (ΔE_{vdW}) to the calculated BE, as shown in Figure 14. Dispersion contributions were referenced to those of adsorbate and model system at infinite separation.

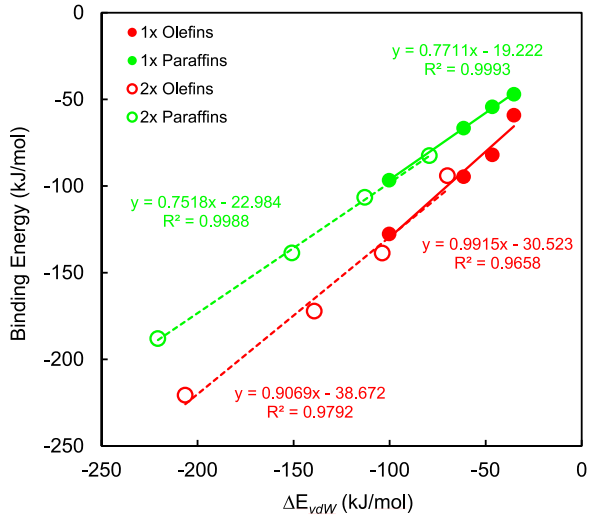

Figure 14. Calculated BEs of olefin (red) and paraffin (green) complexes in monomer and dimer states plotted as a function of the vdW contribution to the energy.

The use of such correlations may be useful in future studies toward estimation of energy barriers for bimolecular reactions such as olefin oligomerization, which is particularly important for zeolitic systems, as computational cost of locating transition states can be steep.

CONCLUSIONS

Automatically generated reaction networks and associated microkinetic models are a powerful tool in analysis, design, and scaleup of important industrial processes and can involve on the order of several hundred or even thousands of elementary steps. Explicit determination of thermodynamic quantities and kinetic parameters for each elementary step is impractical in these systems due to extensive computational time requirements, making it critical that correlations are available, and the scaling relations used are of the highest possible accuracy. Including coverage effects toward accurate estimates of dimer formation energies on BA sites is critical to parameter estimation via scaling relations, as poor estimates of such values can result in distorted potential energy surfaces, greatly affecting predicted reaction rates.

In this work, we report a range of adsorption energies for a wide array of species as monomers and homodimers in acidic and siliceous model systems of the MFI framework. Electronic energies, enthalpies, and free energies of adsorption were calculated for all adsorbates in both systems. Adsorption energies of dimer species were shown to correlate linearly with the corresponding monomer adsorption energies, with the dimer BEs showing slightly different degrees of dependence based on the adsorbate class considered. Class-specific linear scaling relations were developed for adsorption in HZSM-5 materials, while proportional increases (doubling) in monomer BEs were observed for the vast majority of adsorbates in

https://doi.org/10.1021/acs.jpcb.1c02929
J. Phys. Chem. B 2021, 125, 7199−7212

SiZSM-5. Correlations for estimating adsorption energies of monomer and dimer states of paraffins and α-olefins as a function of chain length were developed for HZSM-5 and SiZSM-5 systems. The findings reported in this work provide improvements to the accuracy of existing linear scaling relations and introduce adsorbate-specific relations toward accurate estimates of dimer formation energies.

■ ASSOCIATED CONTENT

Supporting Information

The Supporting Information is available free of charge at https://pubs.acs.org/doi/10.1021/acs.jpcb.1c02929.

All coordinates corresponding to the converged ground states along with the correlations based on enthalpy and free energy (PDF)

■ AUTHOR INFORMATION

Corresponding Author

Linda J. Broadbelt − *Department of Chemical and Biological Engineering, Northwestern University, Evanston, Illinois 60208, United States;* orcid.org/0000-0003-4253-592X; Email: broadbelt@northwestern.edu

Authors

Pavlo Kostetskyy − *Department of Chemical and Biological Engineering, Northwestern University, Evanston, Illinois 60208, United States;* orcid.org/0000-0003-2796-0362

Elsa Koninckx − *Department of Chemical and Biological Engineering, Northwestern University, Evanston, Illinois 60208, United States*

Complete contact information is available at: https://pubs.acs.org/10.1021/acs.jpcb.1c02929

Notes

The authors declare no competing financial interest.

■ ACKNOWLEDGMENTS

This paper is based upon work supported primarily by the National Science Foundation (NSF) GRFP Grant DGE-1842165 and under Cooperative Agreement No. EEC-1647722 and the Belgium American Education Fellowship (BAEF). Any opinions, findings, and conclusions or recommendations expressed in this material are those of the author(s) and do not necessarily reflect the views of the National Science Foundation. This work used the Extreme Science and Engineering Discovery Environment (XSEDE), which is supported by National Science Foundation Grant ACI-1053575. This research was also supported in part through the computational resources and staff contributions provided for the Quest high performance computing facility at Northwestern University which is jointly supported by the Office of the Provost, the Office for Research, and Northwestern University Information Technology. The authors acknowledge Prof. William Schneider (Notre Dame), Prof. Raj Gounder (Purdue), and Mr. Jerry Crum (Notre Dame) for advice with computational details and general discussions.

■ REFERENCES

(1) Weckhuysen, B. M.; Yu, J. H. Recent advances in zeolite chemistry and catalysis. *Chem. Soc. Rev.* **2015**, *44* (20), 7022−7024.

(2) (a) Jiang, N.; Shang, R.; Heijman, S. G. J.; Rietveld, L. C. High-silica zeolites for adsorption of organic micro-pollutants in water treatment: A review. *Water Res.* **2018**, *144*, 145−161. (b) Kesraouiouki, S.; Cheeseman, C. R.; Perry, R. Natural Zeolite Utilization in Pollution-Control - A Review of Applications to Metals Effluents. *J. Chem. Technol. Biotechnol.* **1994**, *59* (2), 121−126.

(3) Suib, S. L. Handbook of zeolite science and technology. *Science* **2003**, *302* (5649), 1335−1336.

(4) (a) Di Iorio, J. R.; Hoffman, A. J.; Nimlos, C. T.; Nystrom, S.; Hibbitts, D.; Gounder, R. Mechanistic origins of the high-pressure inhibition of methanol dehydration rates in small-pore acidic zeolites. *J. Catal.* **2019**, *380*, 161−177. (b) Di Iorio, J. R.; Nimlos, C. T.; Gounder, R. Introducing Catalytic Diversity into Single-Site Chabazite Zeolites of Fixed Composition via Synthetic Control of Active Site Proximity. *ACS Catal.* **2017**, *7* (10), 6663−6674. (c) Hoffman, A. J.; Bates, J. S.; Di Iorio, J. R.; Nystrom, S. V.; Nimlos, C. T.; Gounder, R.; Hibbitts, D. Rigid Arrangements of Ionic Charge in Zeolite Frameworks Conferred by Specific Aluminum Distributions Preferentially Stabilize Alkanol Dehydration Transition States. *Angew. Chem., Int. Ed.* **2020**, *59* (42), 18686−18694. (d) Rodriguez-Fernandez, A.; Di Iorio, J. R.; Paris, C.; Boronat, M.; Corma, A.; Roman-Leshkov, Y.; Moliner, M. Selective active site placement in Lewis acid zeolites and implications for catalysis of oxygenated compounds. *Chemical Science* **2020**, *11* (37), 10225−10235. (e) Teixeira, I. F.; Lo, B. T. W.; Kostetskyy, P.; Stamatakis, M.; Ye, L.; Tang, C. C.; Mpourmpakis, G.; Tsang, S. C. E. From Biomass-Derived Furans to Aromatics with Ethanol over Zeolite. *Angew. Chem., Int. Ed.* **2016**, *55* (42), 13061−13066. (f) Teixeira, I. F.; Lo, B. T. W.; Kostetskyy, P.; Ye, L.; Tang, C. C.; Mpourmpakis, G.; Tsang, S. C. E. Direct Catalytic Conversion of Biomass-Derived Furan and Ethanol to Ethylbenzene. *ACS Catal.* **2018**, *8* (3), 1843−1850.

(5) (a) Wang, K.; Huang, X.; Li, D. B. Hollow ZSM-5 zeolite grass ball catalyst in methane dehydroaromatization: One-step synthesis and the exceptional catalytic performance. *Appl. Catal., A* **2018**, *556*, 10−19. (b) Li, Q. Y.; Zhang, F. Q.; Jarvis, J.; He, P.; Yung, M. M.; Wang, A. G.; Zhao, K.; Song, H. Investigation on the light alkanes aromatization over Zn and Ga modified HZSM-5 catalysts in the presence of methane. *Fuel* **2018**, *219*, 331−339. (c) Rahimi, N.; Karimzadeh, R. Catalytic cracking of hydrocarbons over modified ZSM-5 zeolites to produce light olefins: A review. *Appl. Catal., A* **2011**, *398* (1−2), 1−17.

(6) Baerlocher, C.; McCusker, L. B. Database of Zeolite Structures (accessed August 2020). http://www.iza-structure.org/databases/.

(7) Burton, A. W.; Zones, S. I.; Elomari, S. The chemistry of phase selectivity in the synthesis of high-silica zeolites. *Curr. Opin. Colloid Interface Sci.* **2005**, *10* (5−6), 211−219.

(8) (a) Dunne, J. A.; Mariwala, R.; Rao, M.; Sircar, S.; Gorte, R. J.; Myers, A. L. Calorimetric heats of adsorption and adsorption isotherms 0.1. O_2, N_2, Ar, CO_2, CH_4, C_2H_6 and SF_6 on silicalite. *Langmuir* **1996**, *12* (24), 5888−5895. (b) Dunne, J. A.; Rao, M.; Sircar, S.; Gorte, R. J.; Myers, A. L. Calorimetric heats of adsorption and adsorption isotherms 0.2. O_2, N_2, Ar, CO_2, CH_4, C_2H_6, and SF_6 on NaX, H-ZSM-5, and Na-ZSM-5 zeolites. *Langmuir* **1996**, *12* (24), 5896−5904.

(9) Lee, C. C.; Gorte, R. J.; Farneth, W. E. Calorimetric study of alcohol and nitrile adsorption complexes in H-ZSM-5. *J. Phys. Chem. B* **1997**, *101* (19), 3811−3817.

(10) Savitz, S.; Siperstein, F.; Gorte, R. J.; Myers, A. L. Calorimetric study of adsorption of alkanes in high-silica zeolites. *J. Phys. Chem. B* **1998**, *102* (35), 6865−6872.

(11) Chempath, S.; Denayer, J. F. M.; De Meyer, K. M. A.; Baron, G. V.; Snurr, R. Q. Adsorption of liquid-phase alkane mixtures in silicalite: Simulations and experiment. *Langmuir* **2004**, *20* (1), 150−156.

(12) (a) Eder, F.; Lercher, J. A. Alkane sorption in molecular sieves: The contribution of ordering, intermolecular interactions, and sorption on Bronsted acid sites. *Zeolites* **1997**, *18* (1), 75−81. (b) Eder, F.; Stockenhuber, M.; Lercher, J. A. Bronsted acid site and pore controlled siting of alkane sorption in acidic molecular sieves. *J. Phys. Chem. B* **1997**, *101* (27), 5414−5419. (c) Mukti, R. R.; Jentys, A.; Lercher, J. A. Orientation of alkyl-substituted aromatic molecules

during sorption in the pores of WZSM-5 zeolites. *J. Phys. Chem. C* **2007**, *111* (10), 3973−3980. (d) Narbeshuber, T. F.; Vinek, H.; Lercher, J. A. Monomolecular conversion of light alkanes over H-ZSM-5. *J. Catal.* **1995**, *157* (2), 388−395.

(13) (a) Ison, A.; Gorte, R. J. The Adsorption of Methanol and Water on H-ZSM-5. *J. Catal.* **1984**, *89* (1), 150−158. (b) Parrillo, D. J.; Gorte, R. J. Characterization of Acidity in H-ZSM-5, H-ZSM-12, H-Mordenite, and H-Y Using Microcalorimetry. *J. Phys. Chem.* **1993**, *97* (34), 8786−8792. (c) Farneth, W. E.; Gorte, R. J. Methods for Characterizing Zeolite Acidity. *Chem. Rev.* **1995**, *95* (3), 615−635. (d) Savitz, S.; Myers, A. L.; Gorte, R. J. Calorimetric investigation of CO and N_2 for characterization of acidity in zeolite H-MFI. *J. Phys. Chem. B* **1999**, *103* (18), 3687−3690.

(14) Kotrel, S.; Rosynek, M. P.; Lunsford, J. H. Intrinsic catalytic cracking activity of hexane over H-ZSM-5, H-beta and H-Y zeolites. *J. Phys. Chem. B* **1999**, *103* (5), 818−824.

(15) Knott, B. C.; Nimlos, C. T.; Robichaud, D. J.; Nimlos, M. R.; Kim, S.; Gounder, R. Consideration of the Aluminum Distribution in Zeolites in Theoretical and Experimental Catalysis Research. *ACS Catal.* **2018**, *8* (2), 770−784.

(16) Zhang, N.; Liu, C. L.; Ma, J. H.; Li, R. F.; Jiao, H. J. Determining the structures, acidity and adsorption properties of Al substituted HZSM-5. *Phys. Chem. Chem. Phys.* **2019**, *21* (34), 18758−18768.

(17) Richardeau, D.; Joly, G.; Canaff, C.; Magnoux, P.; Guisnet, M.; Thomas, M.; Nicolaos, A. Adsorption and reaction over HFAU zeolites of thiophene in liquid hydrocarbon solutions. *Appl. Catal., A* **2004**, *263* (1), 49−61.

(18) (a) Gounder, R.; Jones, A. J.; Carr, R. T.; Iglesia, E. Solvation and acid strength effects on catalysis by faujasite zeolites. *J. Catal.* **2012**, *286*, 214−223. (b) Jones, A. J.; Zones, S. I.; Iglesia, E. Implications of Transition State Confinement within Small Voids for Acid Catalysis. *J. Phys. Chem. C* **2014**, *118* (31), 17787−17800.

(19) Kostestkyy, P.; Maheswari, J. P.; Mpourmpakis, G. Understanding the Importance of Carbenium Ions in the Conversion of Biomass-Derived Alcohols with First-Principles Calculations. *J. Phys. Chem. C* **2015**, *119* (28), 16139−16147.

(20) Ban, S.; Van Laak, A.; De Jongh, P. E.; Van der Eerden, J.; Vlugt, T. J. H. Adsorption selectivity of benzene/propene mixtures for various zeolites. *J. Phys. Chem. C* **2007**, *111* (46), 17241−17248.

(21) Vernuccio, S.; Bickel, E. E.; Gounder, R.; Broadbelt, L. J. Microkinetic Model of Propylene Oligomerization on Bronsted Acidic Zeolites at Low Conversion. *ACS Catal.* **2019**, *9* (10), 8996−9008.

(22) (a) Chiang, H.; Bhan, A. Catalytic consequences of hydroxyl group location on the rate and mechanism of parallel dehydration reactions of ethanol over acidic zeolites. *J. Catal.* **2010**, *271* (2), 251−261. (b) Zygmunt, S. A.; Curtiss, L. A.; Iton, L. E. Protonation of an H_2O dimer by a zeolitic Bronsted acid site. *J. Phys. Chem. B* **2001**, *105* (15), 3034−3038. (c) Jungsuttiwong, S.; Limtrakul, J.; Truong, T. N. Theoretical study of modes of adsorption of water dimer on H-ZSM-5 and H-Faujasite zeolites. *J. Phys. Chem. B* **2005**, *109* (27), 13342−13351. (d) Zhi, Y. C.; Shi, H.; Mu, L. Y.; Liu, Y.; Mei, D. H.; Camaioni, D. M.; Lercher, J. A. Dehydration Pathways of 1-Propanol on HZSM-5 in the Presence and Absence of Water. *J. Am. Chem. Soc.* **2015**, *137* (50), 15781−15794. (e) Olson, D. H.; Zygmunt, S. A.; Erhardt, M. K.; Curtiss, L. A.; Iton, L. E. Evidence for dimeric and tetrameric water clusters in HZSM-5. *Zeolites* **1997**, *18* (5−6), 347−349.

(23) Bedard, J.; Chiang, H.; Bhan, A. Kinetics and mechanism of acetic acid esterification with ethanol on zeolites. *J. Catal.* **2012**, *290*, 210−219.

(24) (a) De Moor, B. A.; Reyniers, M. F.; Gobin, O. C.; Lercher, J. A.; Marin, G. B. Adsorption of C2-C8 n-Alkanes in Zeolites. *J. Phys. Chem. C* **2011**, *115* (4), 1204−1219. (b) Nguyen, C. M.; De Moor, B. A.; Reyniers, M. F.; Marin, G. B. Physisorption and Chemisorption of Linear Alkenes in Zeolites: A Combined QM-Pot(MP2//B3LYP:-GULP)-Statistical Thermodynamics Study. *J. Phys. Chem. C* **2011**, *115* (48), 23831−23847.

(25) John, M.; Alexopoulos, K.; Reyniers, M. F.; Marin, G. B. First-Principles Kinetic Study on the Effect of the Zeolite Framework on 1-Butanol Dehydration. *ACS Catal.* **2016**, *6* (7), 4081−4094.

(26) (a) Kresse, G.; Furthmuller, J. Efficiency of ab-initio total energy calculations for metals and semiconductors using a plane-wave basis set. *Comput. Mater. Sci.* **1996**, *6* (1), 15−50. (b) Kresse, G.; Furthmuller, J. Efficient iterative schemes for ab initio total-energy calculations using a plane-wave basis set. *Phys. Rev. B: Condens. Matter Mater. Phys.* **1996**, *54* (16), 11169−11186.

(27) (a) Kresse, G.; Joubert, D. From ultrasoft pseudopotentials to the projector augmented-wave method. *Phys. Rev. B: Condens. Matter Mater. Phys.* **1999**, *59* (3), 1758−1775. (b) Blochl, P. E. Projector Augmented-Wave Method. *Phys. Rev. B: Condens. Matter Mater. Phys.* **1994**, *50* (24), 17953−17979.

(28) (a) Grimme, S.; Ehrlich, S.; Goerigk, L. Effect of the Damping Function in Dispersion Corrected Density Functional Theory. *J. Comput. Chem.* **2011**, *32* (7), 1456−1465. (b) Grimme, S.; Antony, J.; Ehrlich, S.; Krieg, H. A consistent and accurate ab initio parametrization of density functional dispersion correction (DFT-D) for the 94 elements H-Pu. *J. Chem. Phys.* **2010**, *132* (15), 154104.

(29) (a) Alvaradoswaisgood, A. E.; Barr, M. K.; Hay, P. J.; Redondo, A. Ab-Initio Quantumm Chemical Calculations of Aluminum Substitution in Zeolite ZSM-5. *J. Phys. Chem.* **1991**, *95* (24), 10031−10036. (b) Ghorbanpour, A.; Rimer, J. D.; Grabow, L. C. Computational Assessment of the Dominant Factors Governing the Mechanism of Methanol Dehydration over H-ZSM-5 with Heterogeneous Aluminum Distribution. *ACS Catal.* **2016**, *6* (4), 2287−2298.

(30) (a) Limtrakul, J.; Chuichay, P.; Nokbin, S. Effect of high coverages on proton transfer in the zeolite/water system. *J. Mol. Struct.* **2001**, *560* (1−3), 169−177. (b) Ryder, J. A.; Chakraborty, A. K.; Bell, A. T. Density functional theory study of proton mobility in zeolites: Proton migration and hydrogen exchange in ZSM-5. *J. Phys. Chem. B* **2000**, *104* (30), 6998−7011.

(31) (a) Tabor, E.; Bernauer, M.; Wichterlova, B.; Dedecek, J. Enhancement of propene oligomerization and aromatization by proximate protons in zeolites; FTIR study of the reaction pathway in ZSM-5. *Catal. Sci. Technol.* **2019**, *9* (16), 4262−4275. (b) Chen, G. W.; Liu, H.; Fadaeerayeni, S.; Shan, J. J.; Xing, A. H.; Cheng, J. H.; Wang, H.; Xiang, Y. Z. Tuning the reactivity of ethylene oligomerization by HZSM-5 framework Al(f)proximity. *Catal. Sci. Technol.* **2020**, *10* (12), 4019−4029.

(32) Loewenstein, W. The Distribution of Aluminum in the Tetrahedra of Silicates and Aluminates. *Am. Mineral.* **1954**, *39* (1−2), 92−96.

(33) Linstrom, P. J.; Mallard, W. G. The NIST Chemistry WebBook: A chemical data resource on the internet. *J. Chem. Eng. Data* **2001**, *46* (5), 1059−1063.

(34) Narbeshuber, T. F.; Brait, A.; Seshan, K.; Lercher, J. A. Dehydrogenation of light alkanes over zeolites. *J. Catal.* **1997**, *172* (1), 127−136.

(35) (a) Piccini, G.; Alessio, M.; Sauer, J.; Zhi, Y. C.; Liu, Y.; Kolvenbach, R.; Jentys, A.; Lercher, J. A. Accurate Adsorption Thermodynamics of Small Alkanes in Zeolites. Ab initio Theory and Experiment for H-Chabazite. *J. Phys. Chem. C* **2015**, *119* (11), 6128−6137. (b) Collinge, G.; Yuk, S. F.; Nguyen, M. T.; Lee, M. S.; Glezakou, V. A.; Rousseau, R. Effect of Collective Dynamics and Anharmonicity on Entropy in Heterogenous Catalysis: Building the Case for Advanced Molecular Simulations. *ACS Catal.* **2020**, *10* (16), 9236−9260.

(36) (a) Rigby, A. M.; Kramer, G. J.; vanSanten, R. A. Mechanisms of hydrocarbon conversion in zeolites: A quantum mechanical study. *J. Catal.* **1997**, *170* (1), 1−10. (b) Kazansky, V. B. Adsorbed carbocations as transition states in heterogeneous acid catalyzed transformations of hydrocarbons. *Catal. Today* **1999**, *51* (3−4), 419−434. (c) Kazanskii, V. B. The Nature of Adsorbed Carbenium Ions as Active Intermediates in Catalysis by Solid Acids. *Acc. Chem. Res.* **1991**, *24* (12), 379−383.

(37) (a) Rozanska, X.; van Santen, R. A.; Demuth, T.; Hutschka, F.; Hafner, J. A periodic DFT study of isobutene chemisorption in

https://doi.org/10.1021/acs.jpcb.1c02929
J. Phys. Chem. B 2021, 125, 7199−7212

proton-exchanged zeolites: Dependence of reactivity on the zeolite framework structure. *J. Phys. Chem. B* **2003**, *107* (6), 1309−1315. (b) Boronat, M.; Viruela, P. M.; Corma, A. Reaction intermediates in acid catalysis by zeolites: Prediction of the relative tendency to form alkoxides or carbocations as a function of hydrocarbon nature and active site structure. *J. Am. Chem. Soc.* **2004**, *126* (10), 3300−3309.

(38) (a) Plessow, P. N.; Studt, F. Theoretical Insights into the Effect of the Framework on the Initiation Mechanism of the MTO Process. *Catal. Lett.* **2018**, *148* (4), 1246−1253. (b) Fecik, M.; Plessow, P. N.; Studt, F. Simple Scheme to Predict Transition-State Energies of Dehydration Reactions in Zeolites with Relevance to Biomass Conversion. *J. Phys. Chem. C* **2018**, *122* (40), 23062−23067. (c) Fecik, M.; Plessow, P. N.; Studt, F. Influence of Confinement on Barriers for Alkoxide Formation in Acidic Zeolites. *ChemCatChem* **2021**, *13* (10), 2451−2458.

https://doi.org/10.1021/acs.jpcb.1c02929
J. Phys. Chem. B 2021, 125, 7199−7212